LETTER | SEPTEMBER 14 2021

Data-driven surrogates of rotating detonation engine physics with neural ordinary differential equations and high-speed camera footage FREE

J. Koch

Physics of Fluids 33, 091703 (2021)
https://doi.org/10.1063/5.0063624

Physics of Fluids LETTER scitation.org/journal/phf

Data-driven surrogates of rotating detonation engine physics with neural ordinary differential equations and high-speed camera footage

Cite as: Phys. Fluids **33**, 091703 (2021); doi: 10.1063/5.0063624
Submitted: 15 July 2021 · Accepted: 27 August 2021 ·
Published Online: 14 September 2021

J. Koch[a)]

AFFILIATIONS

Independent Researcher, 2727 Revere St., Houston, Texas 77098, USA

[a)]Author to whom correspondence should be addressed: jvkoch0@gmail.com

ABSTRACT

Interacting multi-scale physics in the Rotating Detonation Engine (RDE) lead to diverse nonlinear dynamical behavior, including combustion wave mode-locking, modulation, and bifurcations. Here, surrogate models of the RDE physics, including combustion, injection, and mixing, are sought that can reproduce mode-locked combustion waves through their interactions. These surrogate models are constructed and trained within the context of neural ordinary differential equations evolving through the latent representation of the waves: the traveling wave coordinate $\xi = x - ct + a$. It is shown that the multi-scale nature of the physics can be successfully separated and analyzed separately, providing valuable insight into the fundamental physical processes of the RDE.

The *Rotating Detonation Engine* (RDE) is a novel propulsion or stationary power-producing device that seeks to exploit the advantageous thermodynamic properties of constant-volume combustion through continuously rotating detonation waves.[1] RDEs feature periodic combustion chambers [e.g., an annular combustion chamber, such as the idealized combustor pictured in Fig. 1(a)] with fuel and oxidizer injected at the head-end of the device. One or more traveling combustion waves consume the fuel and oxidizer mixture and expel the exhaust rearwards, producing thrust or otherwise high-enthalpy flow from which work can be extracted. The traveling combustion waves are the result of the highly dissipative, multi-scale, and nonlinear balance physics associated with the RDE: Energy gained through combustion competes with dissipation through exhaust, while the fast combustion process is balanced by (and subject to) the slow physics of injection and mixing.[2–4]

These multi-scale physics pose a significant challenge to the engineering tasks of RDE design, operation, and control. These tasks typically are rooted in high-fidelity computational fluid dynamic simulations with detailed combustor geometry, chemical kinetics, and turbulence models that can properly resolve all associated physical scales present in the RDE (see Cocks *et al.*,[5] for example). Because the physics span several orders of magnitude (from sub-microsecond to milliseconds), these simulations are computationally expensive or intractable. Furthermore, validation of these simulations is difficult because of the lack of well-resolved, low-noise, and relevant data from experiments due to the harsh sensing environment (see Naples *et al.*,[21] for example). However, high-speed camera footage of RDEs [such as the data in Fig. 1(b)] provides a readily obtained and spatially resolved space-time history of the kinematics of the combustion waves. Visible spectrum chemiluminescence does not have a direct quantitative relationship to engineering quantities of interest (pressure or temperature, for example), although many have noted basic qualitative properties of this observable that correlate with fluid properties.[6–9] In general, visible spectrum luminosity is indicative of the temperature of the combustion products.[6]

In this work, chemiluminescence measurements obtained from high-speed camera footage are used to construct *surrogate models* of the multi-scale nonlinear phenomena that contribute to the characteristic traveling wave behavior of RDEs within the context of a specific RDE experiment. The end-use goal of these surrogate models is to provide estimates of physical scales and inform how the interactions of these scales result in the observed behavior. This work is critically enabled by: (i) the observation that steadily propagating rotating detonation waves can be completely described by a system of Ordinary Differential Equations (ODEs) evolving in the traveling wave coordinate $\xi = x - ct + a$, where c is the speed of the assumed right-running wave and a is an arbitrary spatial offset,[10] (ii) the observation that pixel-integrated luminosity is proportional to speed (discussed herein), and (iii) *Neural ODEs* (NODEs) and their generalization;

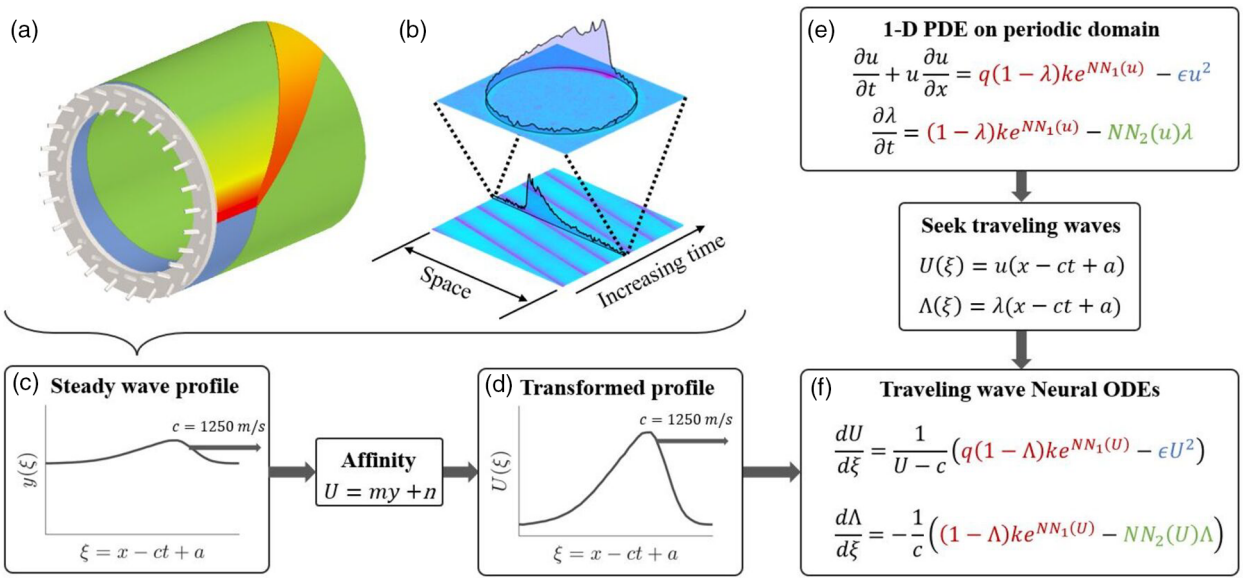

FIG. 1. A notional Rotating Detonation Engine (RDE) is shown in (a). Fuel and oxidizer enter injection ports on the head-end of the device and mix to form a combustible mixture. A number of detonation waves traverse the periodic combustion chamber consuming the newly injected and mixed propellant. The high-enthalpy exhaust flow is expelled rearwards. A common method for observing the detonation wave kinematic behavior is high-speed camera imaging (visible spectrum). High-speed camera footage provides a low-noise and well-resolved space-time history of the traveling waves (b). Snapshots of the annular combustion chamber (128-square pixel images) can be converted into 1D vectors containing the pixel-integrated luminosity about the annulus. These snapshots can be stacked to form a space-time diagram of the experiment. For steady-state operation, multiple camera frames can be phase-averaged to produce a representative steady wave luminosity profile (c). In (e), a wave equation describing the damped-driven activator–inhibitor behavior of the RDE is written for a 1D periodic domain. Trained neural networks are sought to approximate single-step Arrhenius kinetics (shown in red) and the mixing submodel (green) subject to dissipation (blue). In seeking traveling wave solutions, the partial differential equation is transformed to a system of ordinary differential equations (ODEs) evolving through the coordinate $\xi = x - ct + a$ (f). This model is fit to an affine transformation of the high-speed camera footage (d) through auto-differentiation.

Univeral ODEs.[11] A model *activator–inhibitor* dynamical system [Fig. 1(e)] evolving through the traveling wave coordinate ξ is constructed with basic assumptions regarding the essential RDE balance physics [Fig. 1(f)]. Assuming that luminosity is a sufficient surrogate measurement for the *activator* [Figs. 1(c) and 1(d)], this dynamical system is fit to experimentally obtained high-speed camera footage. This type of modeling architecture is chosen over other relevant data-driven methods (see Maulik *et al.*,[12] Massa *et al.*,[13] or Kabanov and Kasimov,[14] for examples) in that the traveling wave structure and physical scales are embedded by construction of the model.

High-speed camera footage from two experiments is presented in this Letter: (i) high-amplitude modulation of two waves and (ii) four steadily propagating combustion waves. The former experiment is used to establish speed-amplitude properties of as-observed luminosity. The latter experiment is the source of data for exploratory model training. Both experiments were performed at the University of Washington High Enthalpy Flow Laboratory with a 76-mm flowpath outside diameter RDE with a mixture of gaseous methane and oxygen. The engine test stand is a closed vacuum chamber with a large exhaust plenum and in-line optical access for direct line-of-sight to the exit of the combustor. A complete description of the test stand experimental apparatus is given in Refs. 15 and 16, respectively. Each experiment was imaged with a Phantom Camera v2511 high speed camera at 240 000 frames per second at a resolution of 128×128 pixels. As shown in Fig. 1(b), the high-speed camera footage from experiments can be manipulated to form space-time diagrams of the wave kinetics. These histories are the primary source of data for this work.

Wave unsteadiness is one of the hallmark features of the RDE. This unsteadiness is manifested as wave modulation, bifurcations to more or fewer waves, and/or chaotic propagation. Figure 2 depicts the space-time history of an experiment immediately after nucleation of a second co-rotating combustion wave (global equivalence ratio of 1.1 and mass flow rate of 90 g/s). In Fig. 2(b), the post-processed high-speed camera footage is shown in the laboratory reference frame. The spatial dimension is normalized to reflect the 2π periodicity of the combustion chamber. In Fig. 2(c), the data in Fig. 2(b) are shifted into the wave-attached reference frame. In this frame, the phase difference between the two waves is highlighted. This phase difference oscillates about π radians. Such modulations are common during the ramp-up or ramp-down of propellant feed during the startup and shutdown transients of experiments.

The oscillations in phase difference of the waves are also accompanied by oscillations in wave speed and observed luminosity. Figure 2(d) shows the evolution of speed through the displayed transient behavior. The relationship between camera-observed luminosity and wave speed is approximately linear, as shown in Fig. 3. Linear speed-amplitude relationships are pervasive in nonlinear wave physics; examples include the Korteweg–de Vries equation[17] and Burgers' equation[18] with each possessing the nonlinear advection term $u\frac{\partial u}{\partial x}$. Thus, the amplitude of this observable is dependent on the speed of the waves; this property should be retained in model construction.

Figure 4 shows a high-speed camera footage from an experiment with four steadily propagating combustion waves (the global equivalence ratio of 0.32 and mass flow rate of 226 g/s). In Fig. 4(b), the

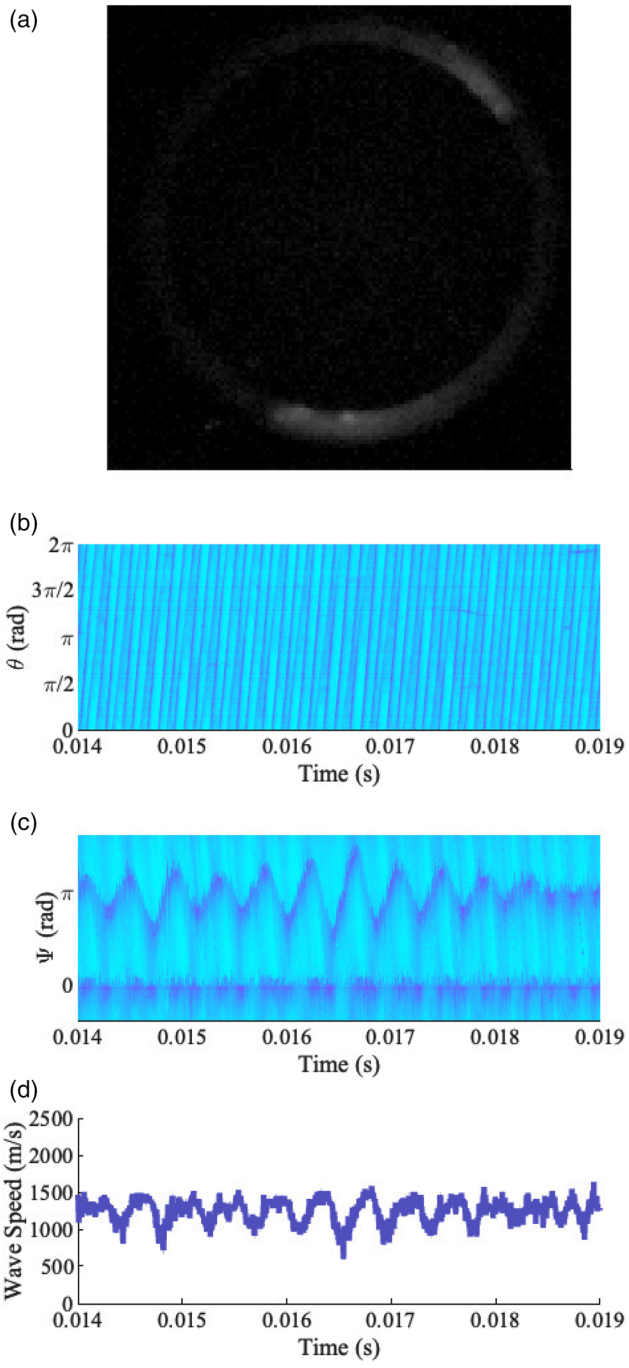

FIG. 2. A high-speed camera frame of an experiment with large-amplitude wave modulation is shown in (a). The space-time history of the waves from this video is shown in (b) in the laboratory reference frame. Shifting the data in (b) into the wave-attached reference frame yields (c) where the evolution of the phase difference, denoted as Ψ, between the waves is clearly observed. In this experiment, the two waves oscillate about a phase difference of π radians. In (d), the speed of the tracked wave in (c) is shown. The global equivalence ratio is 1.1, and the mass flow rate is 90 g/s. Multimedia view: https://doi.org/10.1063/5.0063624.1

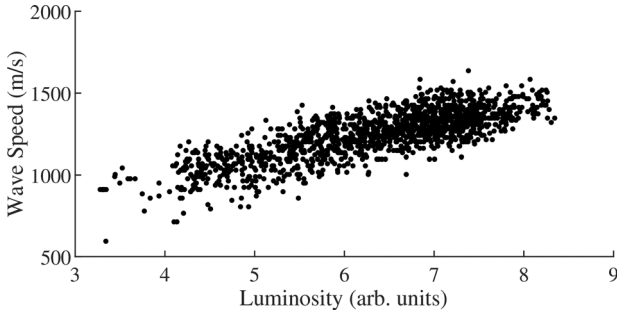

FIG. 3. The relationship between the instantaneous wave speed and camera-observed luminosity is linear. Data points correspond to the wave amplitude along the line $\Psi = 0$ in Fig. 2(b) and the corresponding instantaneous wave speed in Fig. 2(c).

space-time history is shown in the laboratory reference frame. The spatial coordinate bounds correspond to the length of the annular chamber. In Fig. 4(c), an instantaneous circumferential 1D snapshot of the luminosity wave profile [corresponding to the vertical white bar in Fig. 4(b)] is shown. The slopes of the stripes in Fig. 4(b) correspond to the wave speed for this portion of the experiment. For this case, the measured velocity is 1250 m/s. For the given methane-oxygen input mixture, this corresponds to 65% of the theoretical detonation speed at standard temperature and pressure.

Because the waves are approximately steady, a representative wave profile can be obtained by shifting the data into the wave-attached reference frame and averaging in time. This profile is given in Fig. 4(d) (solid line) for one period. This reduced-noise luminosity profile is the training data for this work.

The RDE is a damped-driven activator–inhibitor system. The propagating combustion wave fronts are autosolitons that result from the local balance of nonlinearity (self-steepening of waves), gain (combustion), and dissipation (exhaust) subject to the slow-scale gain recovery (injection and mixing).[4] The *Rotating Detonation Analog*[2] relates mathematical approximations of these physical processes and their associated scales in a compact framework—a two-component 1D partial differential equation—that is amenable to standard analysis techniques,

$$\frac{\partial u}{\partial t} + u\frac{\partial u}{\partial x} = q(1-\lambda)\omega(u) - \varepsilon u^2, \tag{1}$$

$$\frac{\partial \lambda}{\partial t} = (1-\lambda)\omega(u) - \beta(u)\lambda, \tag{2}$$

where $u(x, t)$ is a spatially and temporally variable quantity analogous to specific internal energy, $\lambda(x, t)$ is a combustion progress variable, q is heat release, $\omega(u)$ is the chemical kinetic sub-model, ε is the loss coefficient, and $\beta(u)$ is the injection and mixing sub-model. In general, $\omega(u)$ and $\beta(u)$ are parameterized functions of $u(x, t)$.

This analog system is able to qualitatively reproduce the nonlinear dynamics observed in experiments, including wave mode-locking, modulation, and bifurcations. Additionally, this analog model is built upon the nonlinear advection term $u\frac{\partial u}{\partial x}$ responsible for linear speed-amplitude behavior and shock formation. Thus, expected is that a generalized model of this form can be fit to an affine transformation of the phase-averaged experimental luminosity observations presented in

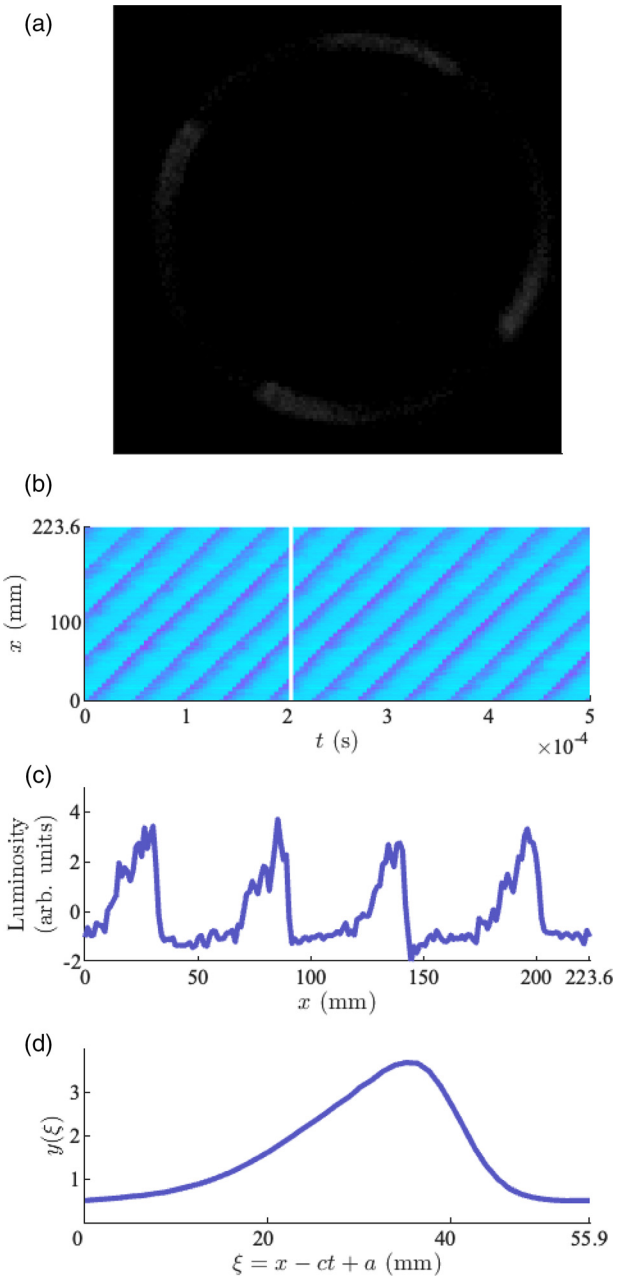

FIG. 4. A high-speed camera frame from an experiment with four mode-locked waves is shown in (a). A short space-time of the waves as recorded by the high-speed camera is shown in (b). In (c), an instantaneous snapshot of the system at $t = 2 \times 10^{-4}$ s is shown exhibiting the characteristic RDE "sawtooth" wave profile. Because these waves are approximately steady, they can be phase-averaged to produce a low-noise representative profile, such as that is shown in (d). The global equivalence ratio is 0.32, and the mass flow rate is 226 g/s. Multimedia view: https://doi.org/10.1063/5.0063624.2

Fig. 4(d). However, the exact functional forms of these physics submodels may be incorrect or otherwise improperly specified. Therefore, instead the following system is fit to the experimental luminosity wave profile,

$$\frac{\partial u}{\partial t} + u\frac{\partial u}{\partial x} = q(1-\lambda)k\exp\left(NN_1(u)\right) - \varepsilon u^2, \tag{3}$$

$$\frac{\partial \lambda}{\partial t} = (1-\lambda)k\exp\left(NN_1(u)\right) - NN_2(u)\lambda, \tag{4}$$

where $k\exp(NN_1)$ is a single-step Arrhenius surrogate model for chemical kinetics with a Neural Network (NN) and NN_2 is the neural network surrogate model for injection and mixing. The Burgers' flux and dissipation terms are unchanged as these functional forms are derived as opposed to modeled.

Equations (3) and (4) are transformed into Ordinary Differential Equations (ODEs) by seeking traveling wave solutions with the transformation into the coordinate $\xi = x - ct + a$. The model form becomes

$$\frac{dU}{d\xi} = \frac{1}{U-c}\left(q(1-\Lambda)k\exp\left(NN_1(U)\right) - \varepsilon U^2\right) = g(U,\Lambda;\theta), \tag{5}$$

$$\frac{d\Lambda}{d\xi} = -\frac{1}{c}\left((1-\Lambda)k\exp\left(NN_1(U)\right) - NN_2(U)\Lambda\right) = h(U,\Lambda;\theta), \tag{6}$$

with $u(x,t) = U(\xi = x - ct + a)$ and $\lambda(x,t) = \Lambda(\xi = x - ct + a)$. The model equations (5) and (6) are now amenable to standard machine learning techniques for dynamical systems. However, instead of evolving through time, here the model evolves through the time-like coordinate ξ.

For consistency, the representative phase-averaged wave profile [Fig. 4(d)] needs to be transformed into ξ. This transformation is done implicitly by setting the spatial offset a to be exactly equivalent to ct; thus, $\xi = x - ct + a = x$. Note that this implicit transformation only holds for individual snapshots of the system but that in the case for steadily propagating waves, each snapshot is identical up to an arbitrary spatial shift.

Neural ODEs evolve a state $\mathbf{z}$ through an independent variable (ξ in this case) through a prescribed input–output mapping defined by a neural network or composite function containing a neural network, f,

$$\mathbf{z}(\xi_{end}) = \mathbf{z}(\xi_0) + \int_{\xi_0}^{\xi_{end}} f(\mathbf{z}(\xi);\theta)d\xi, \tag{7}$$

where θ are the trainable parameters of the model. Equation (7)—an initial value problem—can be solved with standard numerical ODE solvers,

$$\mathbf{z}(\xi_{end}) = \mathrm{ODESolve}(f, \mathbf{z}_0, \xi_0, \xi_{end}; \theta), \tag{8}$$

where $\mathbf{z}_0$ is the initial condition. The model parameters θ are optimized by backpropagating residuals through the numerical ODE solver to provide necessary gradients.

The loss function to be minimized compares the phase-averaged luminosity profile of Fig. 4(d) to numerically integrated neural ODE waveforms. Note that because the only observable is luminosity, or the activator, there is no constraint on Λ dynamics. Furthermore, the necessary translation and scaling of the luminosity data to fit the physical and mathematical assumptions (satisfying Burgers' flux, for example) is unknown. Therefore, in addition to optimizing the model parameters, an affine transformation of the data must also be learned. This is accomplished by encoding a proportionality constant m and offset n into the loss function,

$$\begin{bmatrix} U(\xi) \\ \Lambda(\xi) \end{bmatrix} = \text{ODESolve}\left(\begin{bmatrix} g \\ h \end{bmatrix}, \begin{bmatrix} my_0 + n \\ \Lambda_0 \end{bmatrix}, \xi_0, \xi_{end}; \theta \right), \quad (9)$$

$$\mathscr{L} = \sum_j \left(y(\xi_j) - \frac{U(\xi_j) - n}{m} \right)^2, \quad (10)$$

where $y(\xi)$ is the experimental data, $\xi_0 = 0$ m, $\xi_{end} = 0.0559$ m (length of one period), Λ_0 is a user-specified hyper-parameter setting a reference value for the combustion progress variable ($\Lambda = 0.9$ in this work), and the left-hand side of Eq. (9) represents output data streams for U and Λ on equally spaced evaluation points j corresponding to the training data.

The model was constructed and trained in the Julia computing ecosystem.[19] The ODE solver used was a 5th-order Runge–Kutta integrator. The neural networks used each consist of a single sigmoid-activated layer of dimension 3 and a linear output layer. The Broyden-Fletcher-Goldfarb-Shannon (BFGS) optimization routine was used to select parameters subject to the loss function. For this exploratory study, convergence was deemed sufficient when the error plateaued.

The regression is performed with the knowledge of (i) the wave speed and (ii) the fractional Chapman–Jouguet detonation velocity. For this experiment, the waves traveled at 1250 m/s corresponding to 65% of the theoretical detonation velocity. The RDE analog has a corresponding detonation velocity[20] equal to twice the heat release; $D_{CJ} = 2q$. The heat release parameter is set to $q = 932$ such that $D_{CJ} = 1864$ m/s, matching the detonation velocity of the propellant mixture in the experiment for this fueling condition. The unknown parameters are a, b, ε, and k in addition to the neural network weights. For training, the waveform is flipped such that it appears left-running and the speed is set to $c = -1250$ m/s. This step is taken to ensure that the ODE evolves chemical reactions in a manner consistent with temporal integration. After multiple successful training trials and network architecture permutations, it was found that the neural network approximating the injection and mixing processes defaults to a constant output value without compromising model accuracy. This network has, therefore, been replaced with a single trainable parameter, s, for these results.

Figure 5 shows the reconstruction and continuation of the experimental data with the trained neural ODE model. The trained model parameters are given in Table I. The training data correspond to the discrete plot markers to the left of the vertical black bar. The solid red trace is the neural ODE reconstruction of the data. The green trace corresponds to the combustion progress variable dynamics. The model is successful in reproducing the limit cycle behavior of this experiment, including the unobserved state variable Λ.

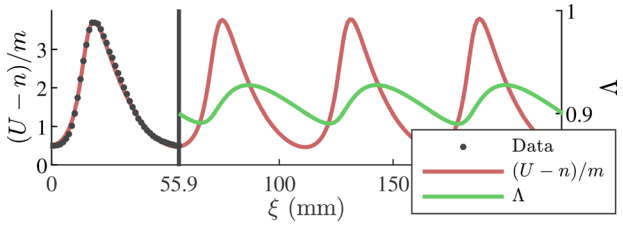

FIG. 5. Experimental luminosity observations are shown to the left of the vertical black bar at 55.9 mm. The reconstruction of the data is given by the under-laid red trace with extrapolation to the right of the black bar. The model output additionally provides an estimate for the combustion progress variable dynamics as shown in green. The neural ODE model is able to successfully reproduce the expected limit cycle behavior.

TABLE I. Trained model parameters.

k	ε	s	m	n
22.17	32 250	3686	2.41	5.55

In addition to reproducing the data, the model can be further dissected to give physical insights about this particular experiment. Figure 6 shows the trained surrogate model for chemical kinetics *based on activation through luminosity*. As expected for an assumed single-step chemical reaction model, the reaction rate increases with luminosity, eventually plateauing in the limit of large luminosity. These reaction rates can be directly compared with another model output; the propellant regeneration rate constant $\tau = 1/s = 2.71 \times 10^{-4}$ s. Thus, the model is able to successfully separate the wave physics into estimates for its constitutive slow (injection and mixing) and fast (combustion) physics.[21]

The RDE possesses a cascade of interacting physical scales that complicate the physics investigation and engineering tasks associated with these engines. In this work, the traveling wave structure of the steady-state behavior of the RDE was exploited to construct and train an interpretable, physics-informed neural ODE system. This model evolves through the traveling wave coordinate $\xi = x - ct + a$ as opposed to coupled space-time dynamics. The resulting model is capable of successfully separating the slow and fast physics directly from

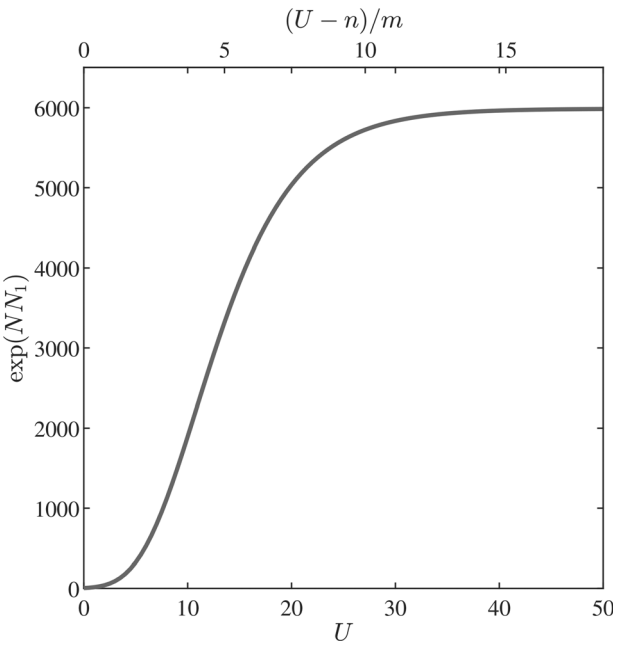

FIG. 6. Response of the surrogate chemical kinetic model to luminosity—the assumed activator. The top abscissa is scaled to match the original data. The bottom abscissa is displayed after the scaling (m) and translation (n).

luminosity measurements as recorded by a standard laboratory-grade high-speed camera. The implications are threefold: (i) the ability to disentangle the physical scales of a particular experiment and/or engine enables the forward analysis tasks of wave existence, stability, and the like, (ii) the estimates of physical scales can be tracked and associated with a specific test article, providing a basis for a rotating detonation engine *digital twin* and *in situ* non-intrusive diagnostics, and (iii) the surrogate models can be re-introduced to the full partial differential equation and used to investigate operability, especially if parameterized by operating conditions.

ACKNOWLEDGMENTS

All experiments were performed at the University of Washington High Enthalpy Flow Laboratory.

The author has no conflicts to disclose.

DATA AVAILABILITY

The data that support the findings of this study are available from the corresponding author upon reasonable request.

REFERENCES

[1]C. A. Nordeen, D. Schwer, F. Schauer, J. Hoke, T. Barber, and B. Cetegen, "Thermodynamic model of a rotating detonation engine," Combust. Explos. Shock Waves **50**, 568–577 (2014).
[2]J. Koch, M. Kurosaka, C. Knowlen, and J. N. Kutz, "Mode-locked rotating detonation waves: Experiments and a model equation," Phys. Rev. E **101**, 013106 (2020).
[3]J. Koch and J. N. Kutz, "Modeling thermodynamic trends of rotating detonation engines," Phys. Fluids **32**, 126102 (2020).
[4]J. Koch, M. Kurosaka, C. Knowlen, and J. N. Kutz, "Multiscale physics of rotating detonation waves: Autosolitons and modulational instabilities," Phys. Rev. E **104**, 024210 (2021).
[5]P. A. Cocks, A. T. Holley, and B. A. Rankin, "High fidelity simulations of a non-premixed rotating detonation engine," in *54th AIAA Aerospace Sciences Meeting* (American Institute of Aeronautics and Astronautics, 2016).
[6]M. Bohon, R. Bluemner, C. Paschereit, and E. Gutmark, "High-speed imaging of wave modes in an RDC," Exp. Therm. Fluid Sci. **102**, 28–37 (2019).
[7]J. W. Bennewitz, B. R. Bigler, S. A. Schumaker, and W. A. Hargus, "Automated image processing method to quantify rotating detonation wave behavior," Rev. Sci. Instrum. **90**, 065106 (2019).
[8]C. L. Journell, R. M. Gejji, I. V. Walters, A. I. Lemcherfi, C. D. Slabaugh, and J. B. Stout, "High-speed diagnostics in a natural gas-air rotating detonation engine," J. Propul. Power **36**, 498–507 (2020).
[9]X. Huang, C. J. Teo, and B. C. Khoo, "Wave mode dynamics in an ethylene-air rotating detonation combustor," AIAA J. **59**, 1808–1823 (2021).
[10]J. Koch, "Data-driven modeling of nonlinear traveling waves," Chaos **31**, 043128 (2021).
[11]C. Rackauckas, Y. Ma, J. Martensen, C. Warner, K. Zubov, R. Supekar, D. Skinner, A. Ramadhan, and A. Edelman, "Universal differential equations for scientific machine learning," arXiv:2001.04385 (2020).
[12]R. Maulik, B. Lusch, and P. Balaprakash, "Reduced-order modeling of advection-dominated systems with recurrent neural networks and convolutional autoencoders," Phys. Fluids **33**, 037106 (2021).
[13]L. Massa, R. Kumar, and P. Ravindran, "Dynamic mode decomposition analysis of detonation waves," Phys. Fluids **24**, 066101 (2012).
[14]D. I. Kabanov and A. R. Kasimov, "Linear stability analysis of detonations via numerical computation and dynamic mode decomposition," Phys. Fluids **30**, 036103 (2018).
[15]J. Koch, M. R. Washington, M. Kurosaka, and C. Knowlen, "Operating characteristics of a ch4/o2 rotating detonation engine in a backpressure controlled facility," in *AIAA Scitech 2019 Forum* (American Institute of Aeronautics and Astronautics, 2019).
[16]J. Koch, L. Chang, C. Upadhye, K. Chau, M. Kurosaka, and C. Knowlen, "Influence of injector-to-annulus area ratio on rotating detonation engine operability," in *AIAA Propulsion and Energy 2019 Forum* (American Institute of Aeronautics and Astronautics, 2019).
[17]R. M. Miura, "The Korteweg-deVries equation: A survey of results," SIAM Rev. **18**, 412–459 (1976).
[18]C. H. Su and C. S. Gardner, "Korteweg-De Vries equation and generalizations. III. Derivation of the Korteweg-De Vries equation and burgers equation," J. Math. Phys. **10**, 536–539 (1969).
[19]C. Rackauckas, M. Innes, Y. Ma, J. Bettencourt, L. White, and V. Dixit, "Diffeqflux.jl—A Julia library for neural differential equations," arXiv:1902.02376 (2019).
[20]A. Majda, "A qualitative model for dynamic combustion," SIAM J. Appl. Math. **41**, 70–93 (1981).
[21]A. Naples, A. M. Knisely, J. Hoke, and F. Schauer, "Infinite line pressure probe and flush transducer measurements in a rotating detonation engine channel," in *AIAA Scitech 2019 Forum* (American Institute of Aeronautics and Astronautics, 2019).